Supplementary Material

Mind the gap: Sex-specific computational modeling reveals distinct mechanisms in bone fracture healing

Laura Lafuente-Gracia, Jamie Madrigal, Pieter Ansoms, Kerri-Ann Norton, Ning Wei, Liesbet Geris, Sarah L. Waters, Aurélie Carlier

S1 Details on the sensitivity analysis

S1.1 Literature-derived perturbation range

The parameter perturbation range used in the global sensitivity analysis was selected based on quantitative sex differences reported in the literature reviewed in Section 1.2. For studies reporting physiological outcomes numerically, or from which approximate values could be extracted from published figures, the relative difference between female and male measurements was calculated as

$$\text{Relative difference } (\%) = \frac{F - M}{M} \times 100,$$

where F and M denote the female and male values, respectively. The reported differences covered a wide range depending on the biological process investigated, but yielded a mean absolute difference of 44.5%. Consequently, a symmetric perturbation interval of $\pm 50\%$ around the baseline parameter values was considered representative of biologically plausible parameter variation while remaining sufficiently broad to capture global sensitivity effects. Table S1 summarizes the literature-derived estimates used to support the selected perturbation range.

Note that the values reported in Table S1 correspond to experimentally measured physiological outcomes (e.g. tissue fractions, cell numbers, or cytokine concentrations) rather than direct estimates of model parameter values (e.g. cellular proliferation, differentiation, or apoptosis rates). These measurements were collected from studies investigating different biological processes, experimental conditions, outcome variables, and (post-fracture) time points. Consequently, they do not constitute a consistent dataset from which sex-specific parameter values can be inferred directly. Nevertheless, they provide a useful indication of the magnitude of sex differences reported across processes relevant to fracture healing.

S1.2 Convergence study

To ensure numerical convergence of the Sobol sensitivity indices, the sensitivity analysis was repeated for increasing sample sizes

$$N = \{2^6, 2^7, 2^8, 2^9, 2^{10}, 2^{11}, 2^{12}, 2^{13}\} = \{64, 128, 256, 512, 1024, 2048, 4096, 8192\}.$$

Table S1: Literature-derived quantitative sex differences used to define the perturbation range for the sensitivity analyses. Relative differences were calculated as $(F - M)/M \times 100$, where F and M denote the female and male values, respectively.

Study	Biological process	Male	Female	Relative difference
Crisostomo et al., 2007 [4]	MSC activation after LPS stimulation	2200	800	-64%
	MSC activation after hypoxia	130	84	-35%
	MSC apoptosis after hypoxia	2.50	1.25	-50%
Strube et al., 2009 [20]	MSC number in femur	1.05	0.08	-92%
	MSC number in tibia	0.48	0.03	-94%
	Osteogenic differentiation	1.20	0.82	-32%
	MSC proliferation	4.5×10^3	3.3×10^3	-27%
	MSC senescence	14.1%	10%	-29%
Katsara et al., 2011 [7]	Growth potential of mMSCs	23%	15%	-35%
Ueno et al., 2011 [23]	M0 macrophages	185	175	-5%
	M1 macrophages	55	30	-45%
	M2 macrophages	55	30	-45%
Haffner-Luntzer et al., 2021 [6]	Bone fraction (10 days)	17%	20%	+18%
	Fibrous tissue fraction (10 days)	42%	56%	+33%
	Cartilage fraction (10 days)	40%	24%	-40%
	Bone fraction (21 days)	45%	45%	0%
	Fibrous tissue fraction (21 days)	52%	52%	0%
	Cartilage fraction (21 days)	0.45%	0.15%	-67%
Andrew et al., 2022 [2]	mSSC numbers after fracture	6000	4500	-25%
	BCSP numbers after fracture	5800	4400	-24%
Molitoris et al., 2024 [14]	M1 macrophages in bone	9%	3%	-67%
	M2 macrophages in bone	0.95%	0.60%	-37%
		Mean absolute difference		**44.5%**

Abbreviations: MSC, mesenchymal stromal cell; mMSC, mouse mesenchymal stromal cell; mSSC, mouse skeletal stem cell; BCSP, bone-cartilage-stromal progenitor cell. *Units:* Values are reported in the original units of the corresponding publication.

Powers of two were selected following standard recommendations for quasi-random Sobol sampling [18]. For each sample size, first-order (S_i) and total-effect (S_{T_i}) indices were computed for all parameters and output metrics. The first-order index measures the fraction of output variance explained by variations in parameter X_i alone, averaged over the uncertainty in all other parameters,

$$S_i = \frac{\mathrm{Var}_{X_i}(\mathrm{E}_{X_{\sim i}}[Y \mid X_i])}{\mathrm{Var}(Y)},$$

where Y denotes the model output. The total-effect index quantifies the overall contribution of parameter X_i, including all interaction effects with other parameters,

$$S_{T_i} = 1 - \frac{\mathrm{Var}_{X_{\sim i}}(\mathrm{E}_{X_i}[Y \mid X_{\sim i}])}{\mathrm{Var}(Y)}.$$

where $X_{\sim i}$ denotes the set of all model parameters except X_i.

Convergence was assessed by comparing the total-effect indices obtained for consecutive values of N. As the sample size increased, the total-effect indices approached stable values, indicating

convergence. The resulting convergence profiles are shown in Figs. S1-S2 and Figs. S3-S4, which group outputs according to metric type (peak value and time-to-peak), as convergence behavior differed between the two metric types.

Convergence was achieved for most outputs at $N = 2^{12} = 4096$, while the time-to-peak of SSPCs (C_s; first row, left panel of Fig. S4) and osteoblasts (C_b; first row, right panel of Fig. S4) required one additional sampling level to stabilize. Although small residual variations remain in a limited number of sensitivity indices, the parameter ranking does not change, indicating that the sensitivity patterns had stabilized. Consequently, $N = 2^{13} = 8192$ was selected for the final sensitivity analysis to ensure convergence of all fifteen output metrics. Given the $D = 37$ model parameters, this corresponded to $N(D + 2) = 8192 \times (37 + 2) = 319\,488$ model evaluations.

S1.3 Results of the global sensitivity analysis ($N = 8192$)

To facilitate comparison across outputs, the results are presented using complementary visualizations. Three-bar plots are used to visualize first-order effects (S_i), total effects (S_{T_i}), and interaction contributions ($S_{T_i} - S_i$) for each output metric. These are grouped into inflammation-related (Figs. S5-S6) and repair-related (Figs. S7-S8) outputs, illustrating common sensitivity patterns within biological phases. Tables are used to summarize the most influential parameters. Only parameters contributing more than 10% of the total variance of a given output metric ($S_{T_i} > 0.1$) are included here. These are presented according to output type, namely peak value (Table S2) and time-to-peak (Table S3), showcasing the different direct- and interaction-driven sensitivity patterns underlying each metric. Both figures and tables rank parameters for each output according to their total-effect index (S_{T_i}) and highlight the independently defined sex-specific parameters. In the tables, for parameters highlighted in blue more than 50% of their total effect arises from interaction effects, that is:

$$\text{Interaction fraction} = \frac{S_{T_i} - S_i}{S_{T_i}} > 0.5$$

The resulting figures and tables are presented below.

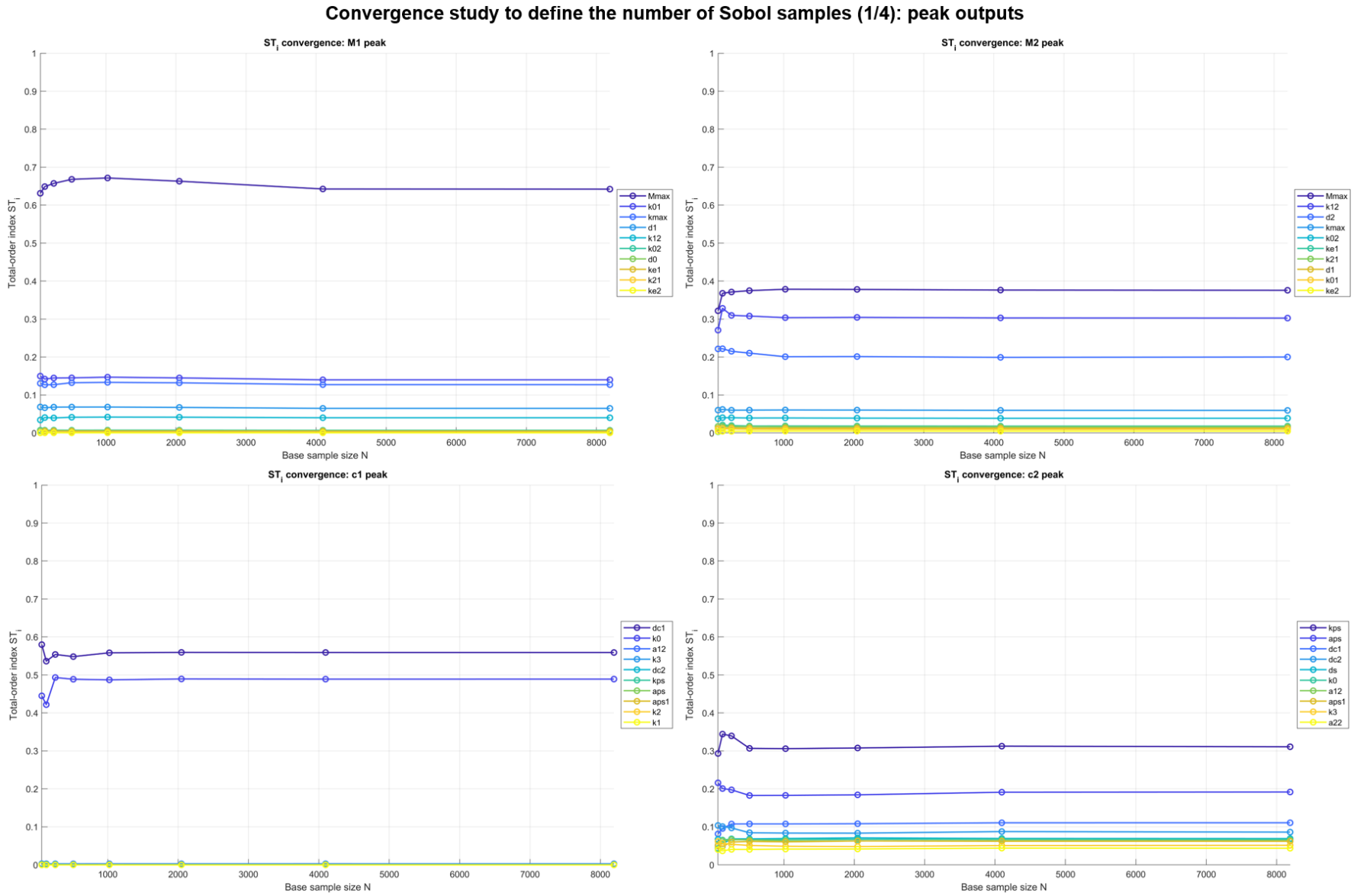


Figure S1: Convergence of total-effect Sobol indices (S_{T_i}) for inflammatory-related peak outputs.

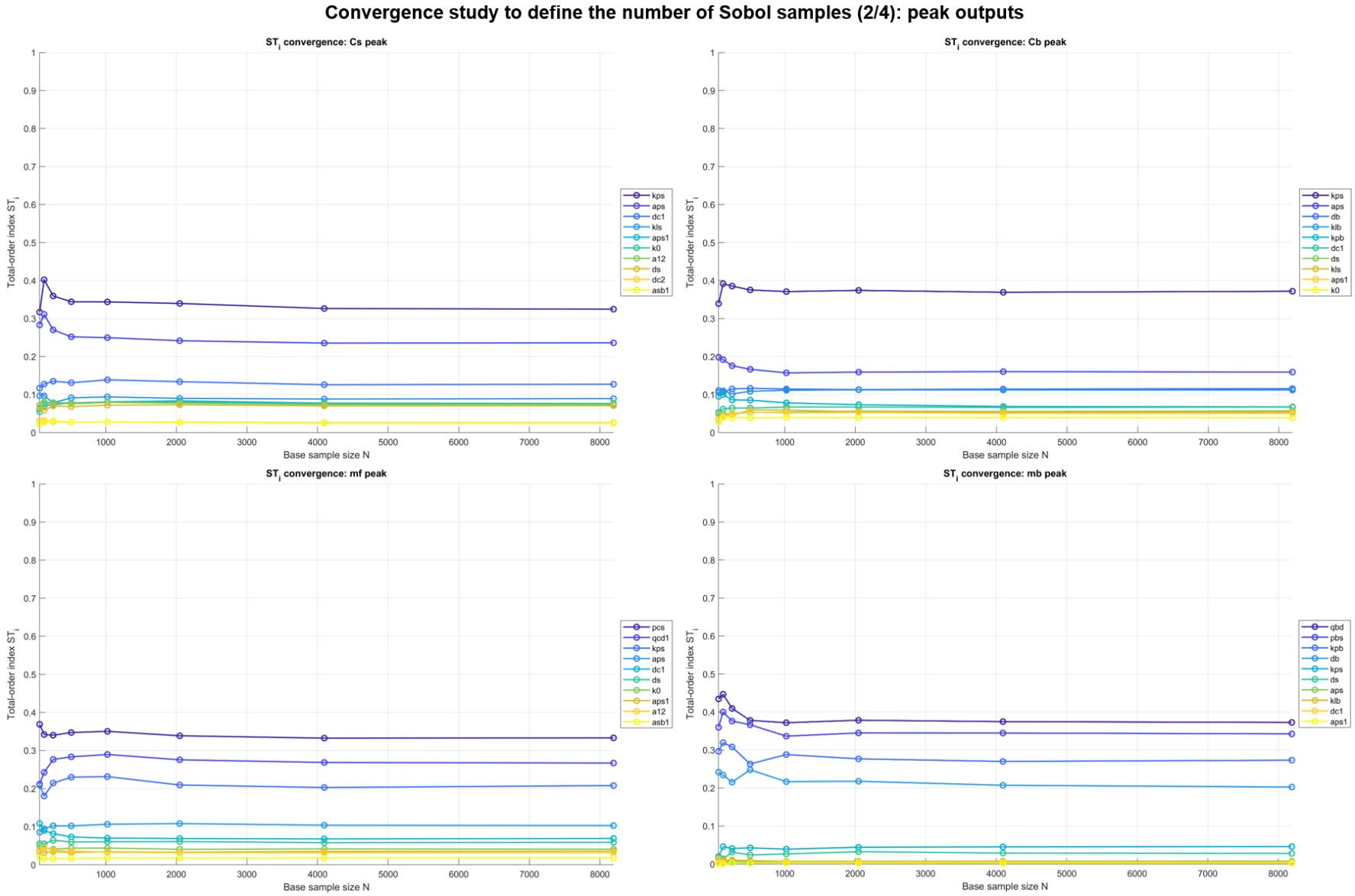


Figure S2: Convergence of total-effect Sobol indices (S_{T_i}) for repair-related peak outputs.

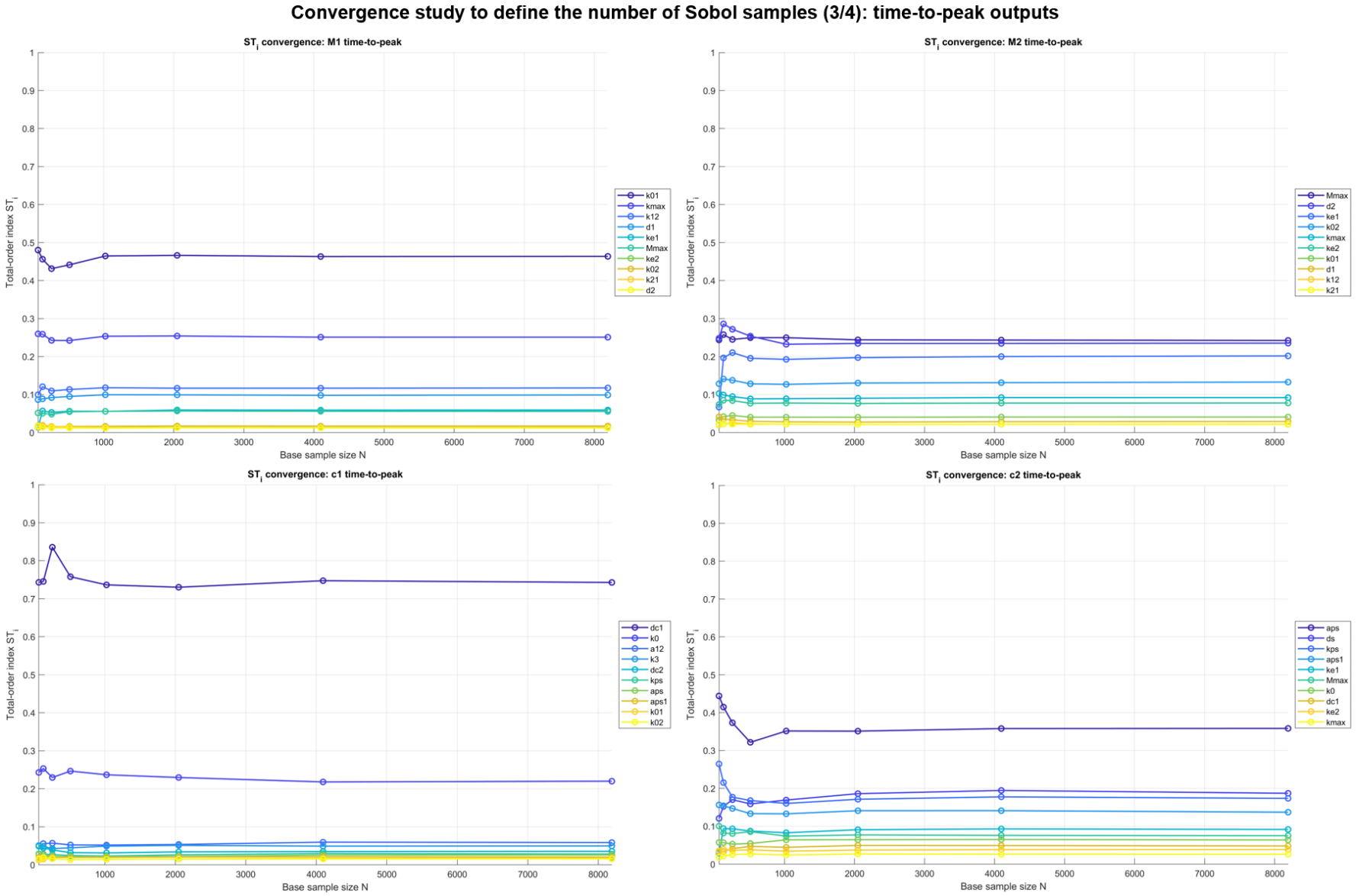


Figure S3: Convergence of total-effect Sobol indices (S_{T_i}) for inflammatory-related time-to-peak outputs.

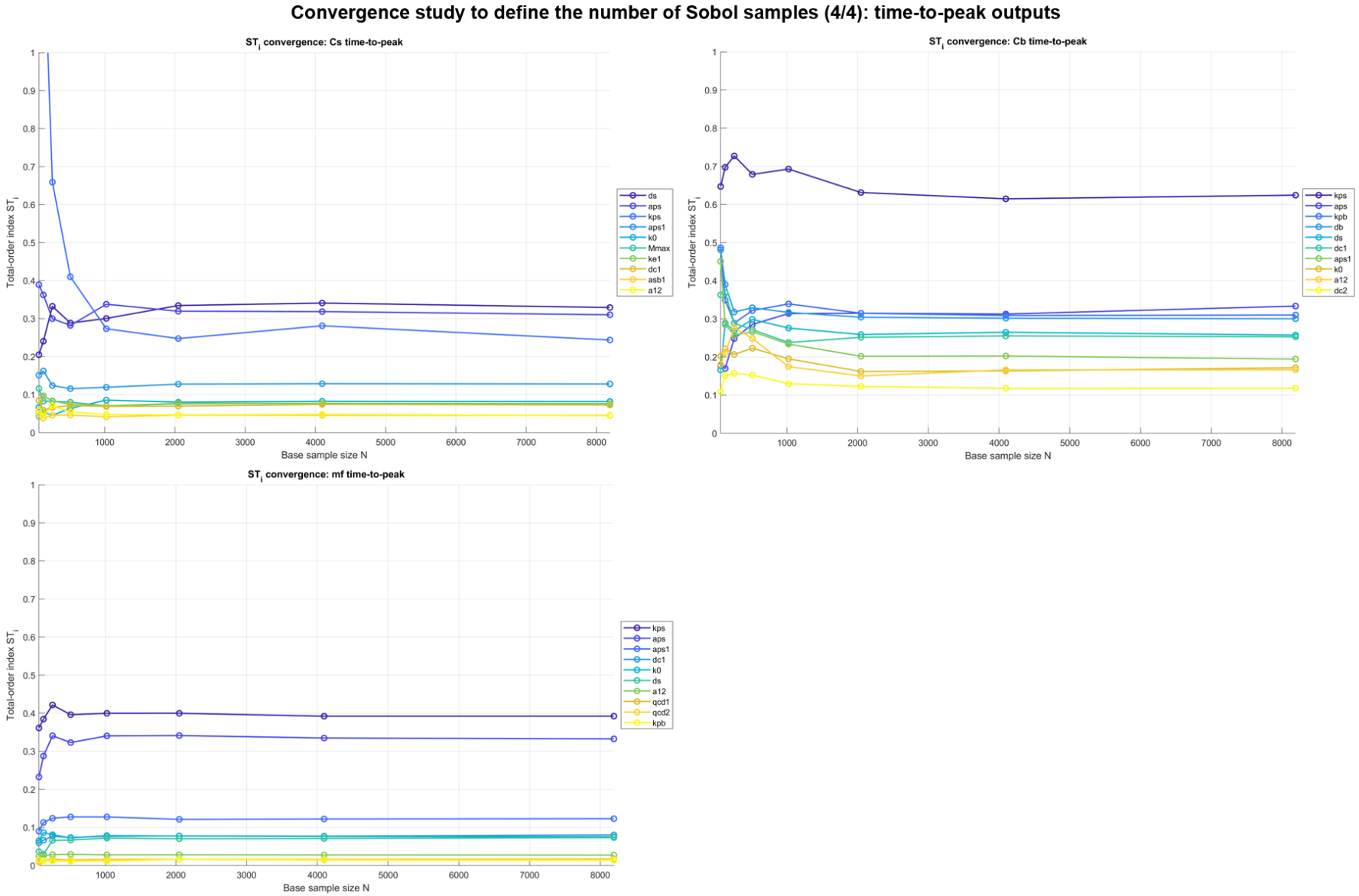


Figure S4: Convergence of total-effect Sobol indices (S_{T_i}) for repair-related time-to-peak outputs. The time-to-peak of woven bone (m_b) was excluded because its maximum was always reached at the final simulation time point.

Table S2: Most influential parameters for peak-value outputs ranked by total-effect Sobol index (S_{T_i}). The interaction contribution was computed as $S_{T_i} - S_i$. Subtractions may not be exact due to rounding. Bold face indicates the parameter is sex-specific, while blue is used to highlight parameters for which more than 50% of the total effect arises from interactions.

Output	Parameter	Description	$\mathbf{S_i}$	$\mathbf{S_{T_i}}$	Interaction
M_1	$\mathbf{M_{max}}$	Maximal macrophage density	0.609	0.643	0.034
	$\mathbf{k_{01}}$	Activation rate of M_0 to M_1	0.133	0.140	0.007
	k_{max}	Maximal macrophage migration rate	0.106	0.127	0.022
M_2	$\mathbf{M_{max}}$	Maximal macrophage density	0.347	0.377	0.030
	k_{12}	Transition rate from M_1 to M_2	0.283	0.304	0.021
	d_2	Apoptosis rate of M_2	0.189	0.201	0.012
c_1	d_{c_1}	Decay rate of c_1	0.506	0.560	0.054
	k_0	Secretion rate of c_1 by debris	0.437	0.490	0.053
c_2	$\mathbf{k_{ps}}$	C_s proliferation rate	0.242	0.309	0.067
	a_{ps}	Effectiveness of c_1 inhibition of C_s proliferation	0.155	0.193	0.038
	d_{c_1}	Decay rate of c_1	0.085	0.113	0.027
C_s	$\mathbf{k_{ps}}$	C_s proliferation rate	0.249	0.319	0.070
	a_{ps}	Effectiveness of c_1 inhibition of C_s proliferation	0.176	0.233	0.057
	d_{c_1}	Decay rate of c_1	0.093	0.132	0.038
C_b	$\mathbf{k_{ps}}$	C_s proliferation rate	0.284	0.377	0.093
	a_{ps}	Effectiveness of c_1 inhibition of C_s proliferation	0.116	0.163	0.047
	$\mathbf{k_{lb}}$	Maximal C_b density	0.082	0.117	0.035
	d_b	Differentiation rate of C_b into osteocytes	0.095	0.116	0.021
m_f	p_{cs}	Fibrocartilage synthesis rate	0.275	0.333	0.058
	q_{cd_1}	Fibrocartilage degradation rate	0.190	0.264	0.073
	$\mathbf{k_{ps}}$	C_s proliferation rate	0.114	0.207	0.093
	a_{ps}	Effectiveness of c_1 inhibition of C_s proliferation	0.055	0.102	0.047
m_b	q_{bd}	Woven bone degradation rate	0.277	0.375	0.098
	p_{bs}	Woven bone synthesis rate	0.265	0.346	0.081
	$\mathbf{k_{pb}}$	C_b proliferation rate	0.118	0.257	0.140
	d_b	Differentiation rate of C_b into osteocytes	0.062	0.204	0.142

Table S3: Most influential parameters for time-to-peak outputs ranked by total-order Sobol index (ST_i). The interaction contribution was computed as $S_{T_i} - S_i$. Subtractions may not be exact due to rounding. Bold face indicates the parameter is sex-specific, while blue is used to highlight parameters for which more than 50% of the total effect arises from interactions.

Output	Parameter	Description	$\mathbf{S_i}$	$\mathbf{S_{T_i}}$	Interaction
M_1	$\mathbf{k_{01}}$	Activation rate of M_0 to M_1	0.437	0.464	0.027
	k_{max}	Maximal macrophage migration rate	0.232	0.249	0.017
	k_{12}	Transition rate from M_1 to M_2	0.103	0.117	0.014
M_2	$\mathbf{M_{max}}$	Maximal macrophage density	0.213	0.244	0.031
	d_2	Apoptosis rate of M_2	0.228	0.238	0.010
	$\mathbf{k_{e_1}}$	Debris removal rate by M_1	0.183	0.203	0.020
	$\mathbf{k_{02}}$	Activation rate of M_0 to M_2	0.116	0.133	0.017
c_1	d_{c_1}	Decay rate of c_1	0.648	0.748	0.100
	k_0	Secretion rate of c_1 by debris	0.137	0.225	0.088
c_2	k_0	Secretion rate of c_1 by debris	0.084	0.570	0.486
	a_{ps}	Effectiveness of c_1 inhibition of C_s proliferation	0.264	0.351	0.087
	$\mathbf{d_s}$	Differentiation rate of C_s into C_b	0.095	0.189	0.095
	$\mathbf{k_{ps}}$	C_s proliferation rate	0.037	0.177	0.140
	a_{ps_1}	Constant enhancement of c_1 to C_s proliferation	0.084	0.134	0.050
C_s	d_{c_2}	Decay rate of c_2	0.031	0.869	0.837
	a_{sb_1}	Effectiveness of c_1 inhibition of C_s differentiation	0.062	0.833	0.771
	a_{12}	Effectiveness of c_2 inhibition of c_1 synthesis	0.074	0.379	0.305
	k_0	Secretion rate of c_1 by debris	0.039	0.367	0.328
	$\mathbf{d_s}$	Differentiation rate of C_s into C_b	0.152	0.339	0.187
	a_{ps}	Effectiveness of c_1 inhibition of C_s proliferation	0.165	0.290	0.125
	$\mathbf{k_{ps}}$	C_s proliferation rate	0.000	0.203	0.203
	a_{ps_1}	Constant enhancement of c_1 to C_s proliferation	0.074	0.143	0.069
C_b	$\mathbf{k_{ps}}$	C_s proliferation rate	0.215	0.655	0.440
	a_{ps}	Effectiveness of c_1 inhibition of C_s proliferation	0.047	0.344	0.297
	d_b	Differentiation rate of C_b into osteocytes	0.026	0.322	0.296
	$\mathbf{k_{pb}}$	C_b proliferation rate	0.024	0.322	0.297
	d_{c_1}	Decay rate of c_1	0.021	0.257	0.236
	$\mathbf{d_s}$	Differentiation rate of C_s into C_b	0.029	0.253	0.223
	a_{ps_1}	Constant enhancement of c_1 to C_s proliferation	0.020	0.196	0.176
	a_{12}	Effectiveness of c_2 inhibition of c_1 synthesis	0.005	0.148	0.143
	k_0	Secretion rate of c_1 by debris	0.017	0.145	0.128
	$\mathbf{k_{lb}}$	Maximal C_b density	0.014	0.122	0.108
	d_{c_2}	Decay rate of c_2	0.000	0.106	0.105
	$\mathbf{k_{e_1}}$	Debris removal rate by M_1	0.000	0.105	0.105
m_f	$\mathbf{k_{ps}}$	C_s proliferation rate	0.333	0.401	0.068
	a_{ps}	Effectiveness of c_1 inhibition of C_s proliferation	0.283	0.332	0.048
	a_{ps_1}	Constant enhancement of c_1 to C_s proliferation	0.105	0.124	0.019

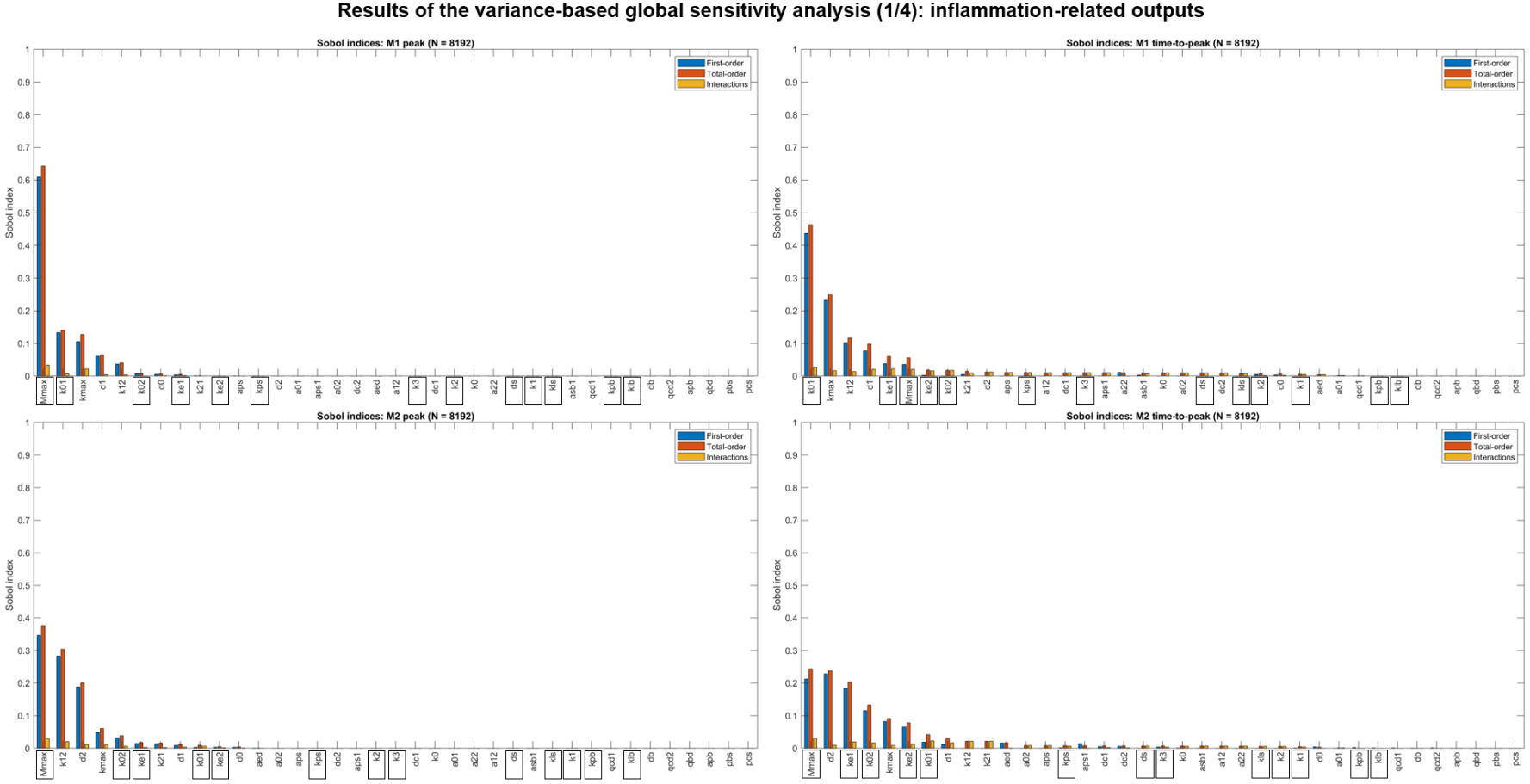


Figure S5: Results of the global sensitivity analysis for inflammatory-related outputs M_1 and M_2. Left: peak-value metric, right: time-to-peak metric. Blue bar: first-order effects (S_i), red bar: total effects (S_{T_i}), yellow bar: interaction effects ($S_{T_i} - S_i$). Sex-specific parameters are indicated in the x-axis.

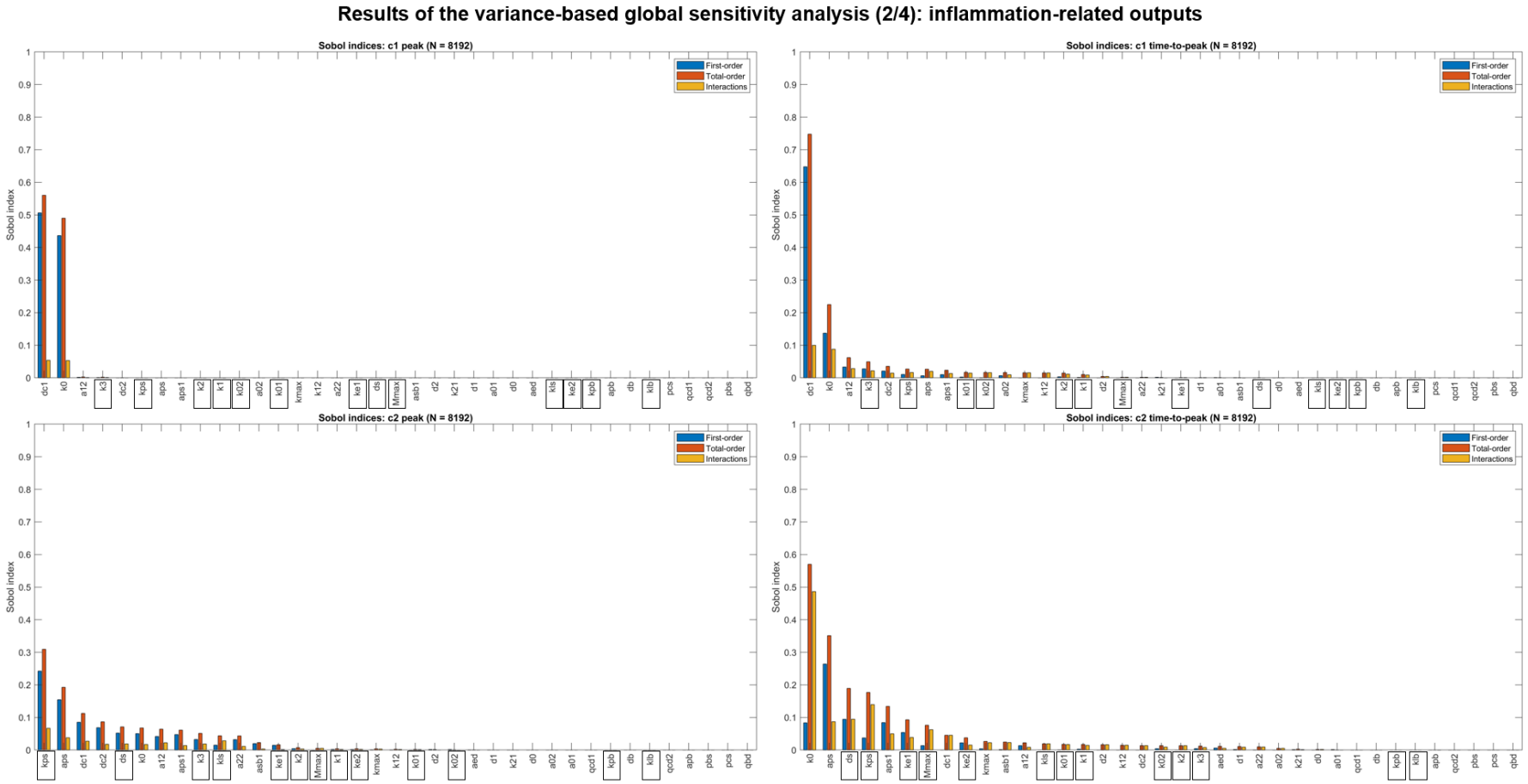


Figure S6: Results of the global sensitivity analysis for inflammatory-related outputs c_1 and c_2. Left: peak-value metric, right: time-to-peak metric. Blue bar: first-order effects (S_i), red bar: total effects (S_{T_i}), yellow bar: interaction effects ($S_{T_i} - S_i$). Sex-specific parameters are indicated in the x-axis.

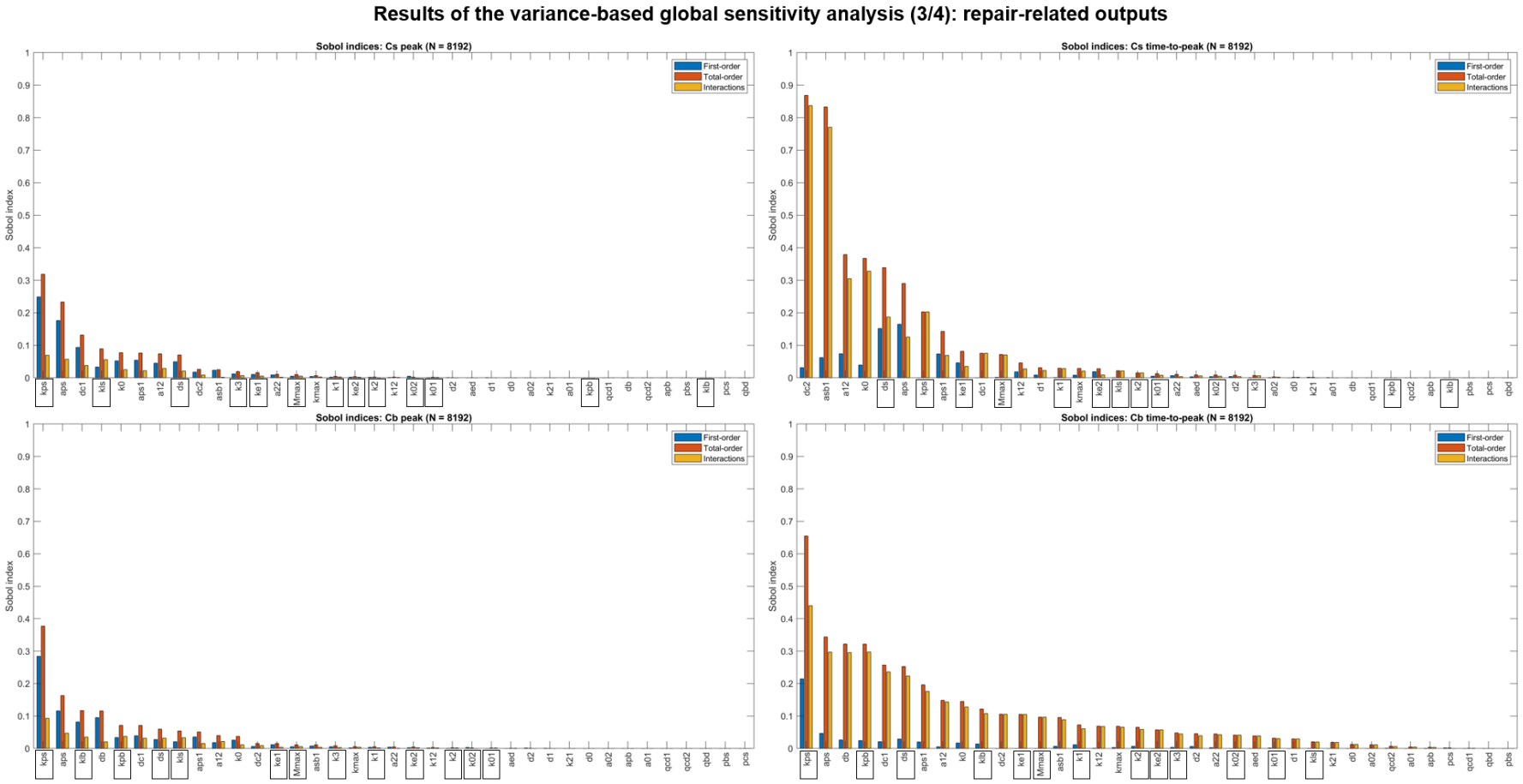


Figure S7: Results of the global sensitivity analysis for repair-related outputs C_s and C_b. Left: peak-value metric, right: time-to-peak metric. Blue bar: first-order effects (S_i), red bar: total effects (S_{T_i}), yellow bar: interaction effects ($S_{T_i} - S_i$). Sex-specific parameters are indicated in the x-axis.

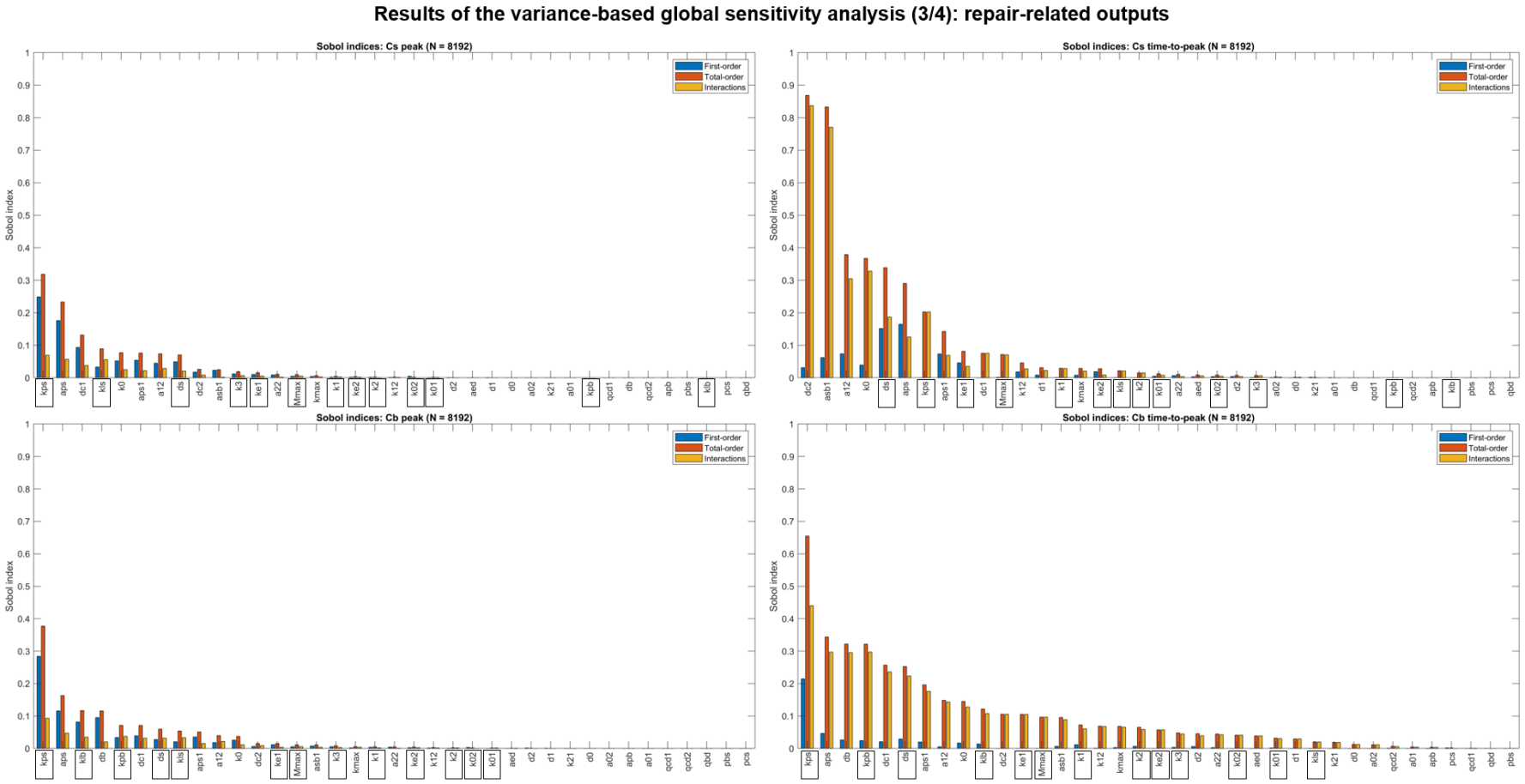


Figure S8: Results of the global sensitivity analysis for repair-related outputs m_f and m_b. Left: peak-value metric, right: time-to-peak metric. Blue bar: first-order effects (S_i), red bar: total effects (S_{T_i}), yellow bar: interaction effects ($S_{T_i} - S_i$). Sex-specific parameters are indicated in the x-axis. The time-to-peak of woven bone (m_b) was excluded because its maximum was always reached at the final simulation time point.

S2 Details on the literature-guided sex-specific parameterization

S2.1 Literature evaluation of model parameters

Each model parameter was evaluated against the literature review presented in Section 1.3 to determine whether these sex differences could be represented through sex-specific parameter values. Table S2.1 summarizes the outcome of this assessment. Parameters were classified according to whether sex-specific evidence was available and used (U; 13 parameters), available but nor directly applicable to the model formulation (A; 1 parameter), contradictory (C; 3 parameters), available only for related cell types (O; 4 parameters), non-available (N; 7 parameters), or non-available due to the model-specific nature of the parameter (M; 9 parameters). Note that the study by Haffner-Luntzer et al. [6] was used as an independent dataset for model validation and was therefore not considered when deriving sex-specific parameter values.

Not all identified sex differences were incorporated into the model. Parameters were left unchanged when the available evidence was contradictory (e.g. woven bone synthesis; p_{bs}), indirect (e.g. macrophage apoptosis inferred from SSPC apoptosis; d_0, d_1 and d_2), or could not be directly translated into the model structure (e.g. fibrocartilage synthesis; p_{cs}). Model-specific parameters such as regulatory thresholds and half-saturation constants also remained unchanged because no direct biological measurements could be mapped to them.

S2.2 Calibration of modification magnitudes

The literature review provided information on the direction of the sex-specific differences (higher or lower in females). Although quantitative sex differences were available for some physiological outcomes, these measurements did not provide direct estimates of the corresponding model parameter values. Consequently, the magnitude of the sex-specific parameter modifications was determined through model calibration.

A first calibration step applied a uniform perturbation of $\pm 50\%$ to all sex-specific parameters. This perturbation magnitude was selected because it corresponds to the parameter range explored in the global sensitivity analysis. However, the resulting repair-phase dynamics exhibited unrealistic behavior, including prolonged persistence of SSPCs and fibrocartilage (see Fig. S9, top row).

A second calibration step applied a uniform perturbation of $\pm 25\%$ to all sex-specific parameters. This produced more realistic repair dynamics, but the resulting SSPC trajectories were inconsistent with the literature evidence indicating lower SSPC numbers in females (see Fig. S9, middle row).

The final calibration therefore combined $\pm 50\%$ modifications for parameters associated with inflammation and macrophage-SSPC crosstalk and $\pm 25\%$ modifications for repair-related parameters. This configuration preserved the literature-supported direction of the reported sex differences while maintaining physiologically plausible healing trajectories (see Fig. S9, bottom row).

Table S4: Literature data that motivated the sex-specific parameterization.

Par.	Description	Evidence for sex differences
k_{e_1}	Debris removal rate by M_1	(U) Enhanced phagocytosis in females [15, 9, 17]
k_{e_2}	Debris removal rate by M_2	(U) Same as k_{e_1}
a_{ed}	Half-saturation of debris	(M)
k_{max}	Maximal macrophage migration rate	(N)
M_{max}	Maximal macrophage density	(U) Increased numbers of macrophages in females [15, 3, 17]
k_{01}	Activation rate of M_0 to M_1	(U) Higher macrophage activation rates in females [9, 3, 19]
k_{02}	Activation rate of M_0 to M_2	(U) Same as k_{01}
a_{01}	Half-saturation of c_1 to activate M_1	(M)
a_{02}	Half-saturation of c_2 to activate M_2	(M)
k_{12}	Transition rate from M_1 to M_2	(C) Not clear whether macrophage polarization is sex-dependent [14, 15]
k_{21}	Transition rate from M_2 to M_1	(C) Same as k_{12}
d_0	Apoptosis rate of M_0	(O) No data for macrophage apoptosis, but SSPC apoptosis was reported higher in female mice [4]
d_1	Apoptosis rate of M_1	(O) Same as d_0
d_2	Apoptosis rate of M_2	(O) Same as d_0
k_0	Secretion rate of c_1 by debris	(N)
k_1	Secretion rate of c_1 by M_1	(U) Greater production of pro-inflammatory cytokines in males [14, 16, 15, 1, 9, 3, 8, 4]
k_2	Secretion rate of c_2 by M_2	(U) Greater production of anti-inflammatory cytokines in females [14, 16, 15, 1, 9, 3, 8, 4]
k_3	Secretion rate of c_2 by C_s	(U) Higher SSPC immunosuppressive capacity in **women** [12, 11], and little to no differences in mice [7, 21]
d_{c_1}	Decay rate of c_1	(N)
d_{c_2}	Decay rate of c_2	(N)
a_{12}	Effectiveness of c_2 inhibition of c_1 synthesis	(M)
a_{22}	Effectiveness of c_2 inhibition of c_2 synthesis	(M)
a_{ps}	Effectiveness of c_1 inhibition of C_s proliferation	(M)
a_{sb_1}	Effectiveness of c_1 inhibition of C_s different.	(M)
a_{pb}	Effectiveness of c_1 inhibition of C_b proliferation	(M)
a_{ps_1}	Constant enhancement of c_1 to C_s proliferation	(M)
k_{ps}	C_s proliferation rate	(U) Higher SSPC proliferation rate in **women** [11] and female mice [24], but lower in female rats [20]
k_{ls}	Maximal SSPC density	(U) Higher numbers of activated SSPCs in male rodents [15, 11, 7, 20]
d_s	Differentiation rate of C_s into C_b	(U) Male mice showed greater differentiation potential across multiple lineages [22, 15, 11, 7, 20, 24, 13]
k_{pb}	C_b proliferation rate	(U) Murine female osteoblasts increased in number due to a higher expression of RANKL and OPG [10, 3]
k_{lb}	Maximal C_b density	(U) Adapted consistently with k_{ls}
d_b	Differentiation rate of C_b into osteocytes	(O) No data for osteoblast differentiation, but male mice SSPC showed greater differentiation potential across multiple lineages [22, 15, 11, 7, 20, 24, 13]
p_{cs}	Fibrocartilage synthesis rate	(A) Greater cartilage formation reported in male-derived SSPC organoids [5], but model combines cartilage and fibrous tissue into a single fibrocartilage compartment
q_{cd_1}	Fibrocartilage degradation rate	(N)
q_{cd_2}	Fibrocartilage degradation rate by osteoclasts	(N)
p_{bs}	Woven bone synthesis rate	(C) Greater bone formation was reported in male mice [10, 13], but also in female mice [15]
q_{bd}	Woven bone degradation rate	(N)

(U) Sex-specific data available and used. (A) Sex-specific data available but not directly applicable to the model. (C) Contradictory data. (O) No sex-specific data, but evidence available for other cell types. (N) No sex-specific data. (M) No direct data due to model-specific parameter.

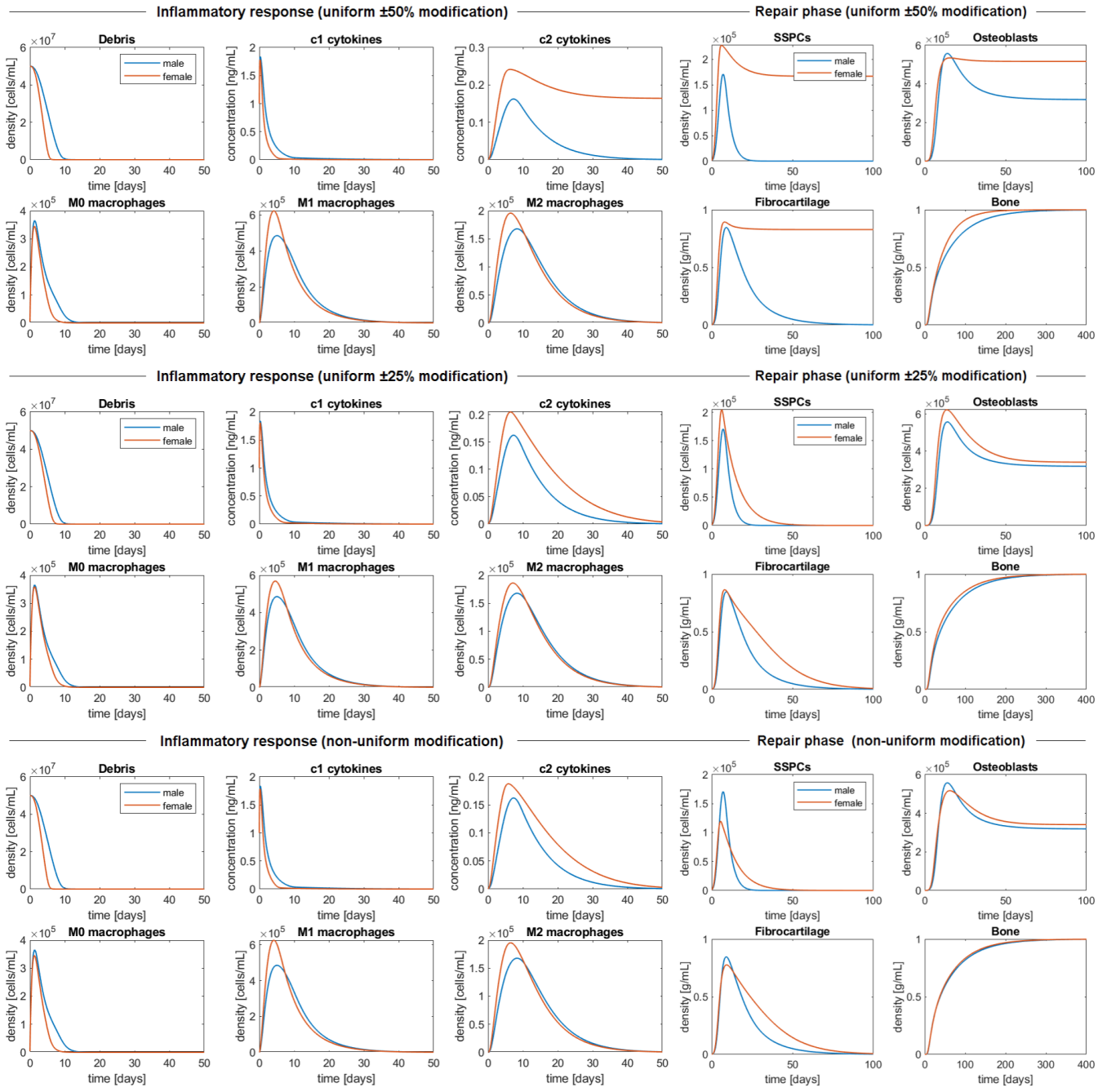


Figure S9: Calibration of sex-specific model parameters. Top row: uniform ±50% modification applied to all sex-specific parameters. Middle row: uniform ±25% modification. Bottom row: combined ±50% (inflammation-related parameters) and ±25% (repair-related parameters) modifications.

S3 Sensitivity of initial conditions

Local sensitivity analyses were conducted to evaluate the influence of uncertainty in the non-zero initial conditions on the simulation outcomes of both the male and female models. The four non-zero initial conditions in the model, namely debris (D), unactivated macrophages (M_0), pro-inflammatory cytokines (c_1), and SSPCs (C_s), were analyzed by scaling their reference values (Table 2) to 10%, 50%, 150%, and 1000%, thereby assessing the robustness of model predictions to uncertainty in the initial fracture environment.

The results show that changes in the initial conditions do not alter the final bone healing outcome, which remains successful regardless of deviations from the reference values for any of the initial conditions in both the male and female models. However, the changes in initial conditions influence the dynamics and time course of the model outcomes. Specifically, both models show robustness (variations $< 5\%$) to small and large changes in the initial conditions of unactivated macrophages and pro-inflammatory cytokines, meaning these initial conditions have only a minor effect on the model dynamics and do not significantly impact the healing process. Therefore, the corresponding figures are omitted for brevity.

In contrast, the initial conditions for debris and SSPCs did affect the simulation outcomes. Due to the mathematical formulation of the model, changes in the SSPC initial conditions do not directly affect the first four variables: that is, debris and macrophage populations (M_0, M_1, and M_2) are not affected by SSPCs. Nevertheless, changes in the SSPC initial conditions influence the dynamics of the remaining outputs, although with limited impact. For small deviations in SSPC initial conditions, the model outcomes showed robustness (variations $< 10\%$), except for the SSPCs population itself, which was moderately impacted, as shown in Figs. S10 and S11. For large deviations, the SSPC initial conditions had a more pronounced effect, particularly on the SSPCs population, where variations exceeded 50%. Despite this, the bone healing outcome remained unaffected.

Finally, the initial debris density exhibited a more pronounced effect on all simulation outcomes for both male and female models, excluding the bone formation predictions. Both small and large changes in the initial conditions of debris led to notable deviations from the corresponding baseline simulation outcomes. The inflammatory response, illustrated in Fig. S12, became more prolonged with amplified peaks and extended plateau phases for larger changes (1000%), particularly in the male model. Smaller changes showed trends similar to the reference outcomes, with the inflammatory response downregulating at similar times. Regarding the repair response, illustrated in Fig. S13, larger changes in the initial debris density (1000%) resulted in prolonged activation of SSPCs and osteoblasts. In the male model, a 1000% increase in debris density led to a longer activation of SSPCs and a more prominent fibrocartilage peak, while osteoblast activation was delayed for the 1000% increase and showed no peak for smaller values of debris initial condition. However, all curves ultimately converged to the same final state as the reference. In the female model, a similar but more subtle effect was observed: a 1000% increase in debris density resulted in a thicker SSPC peak compared to the reference value, but this decayed similarly to the peak resulting from smaller initial changes, leading to similar fibrocartilage peaks across all tested debris initial conditions. While these deviations in the repair process were notable, particularly in the timing and magnitude of peaks and activations, the final prediction of complete bone healing remained consistent across all variations in initial debris conditions, for both male and female models.

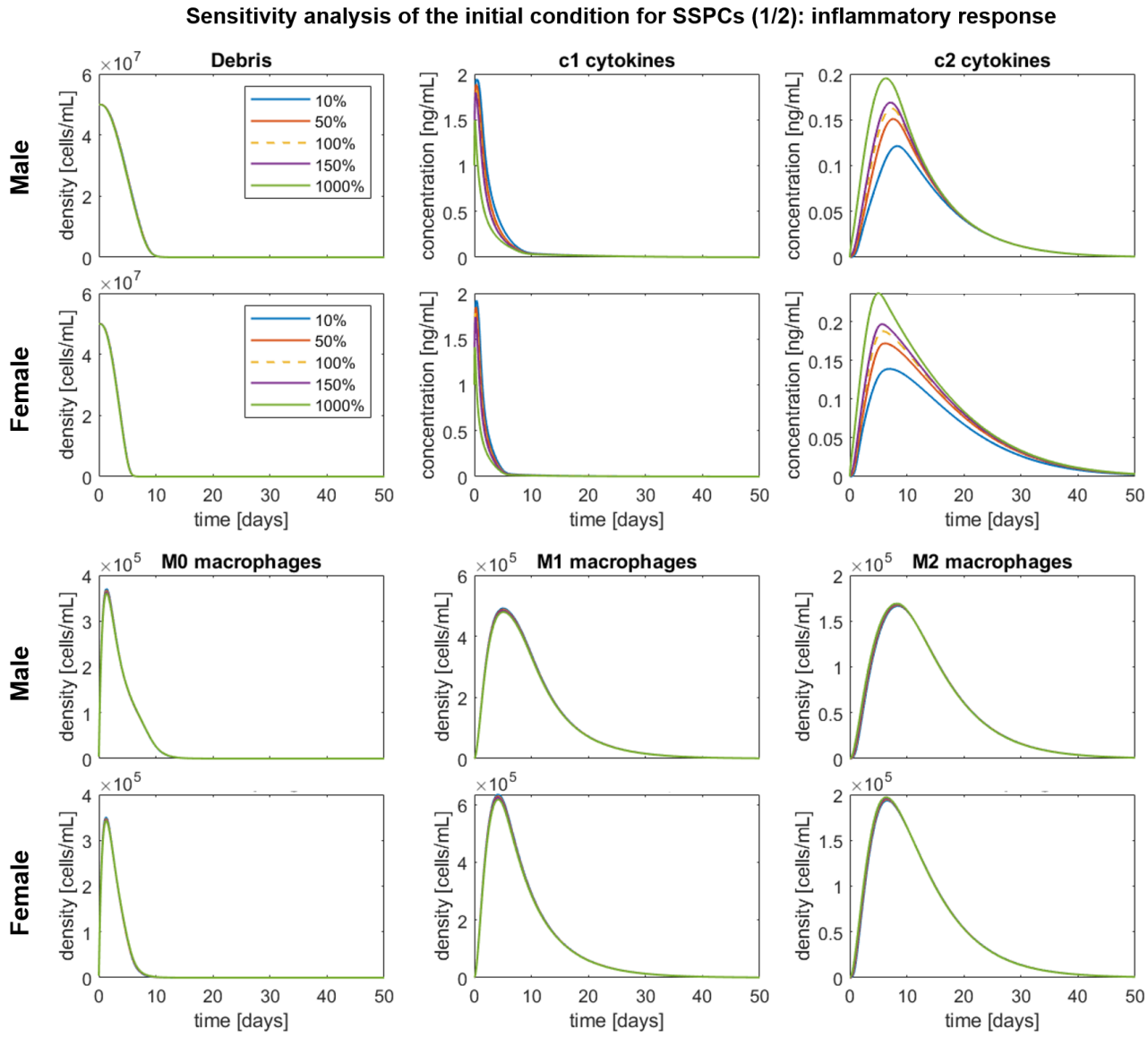


Figure S10: Influence of the initial condition for SSPCs on the inflammatory phase.

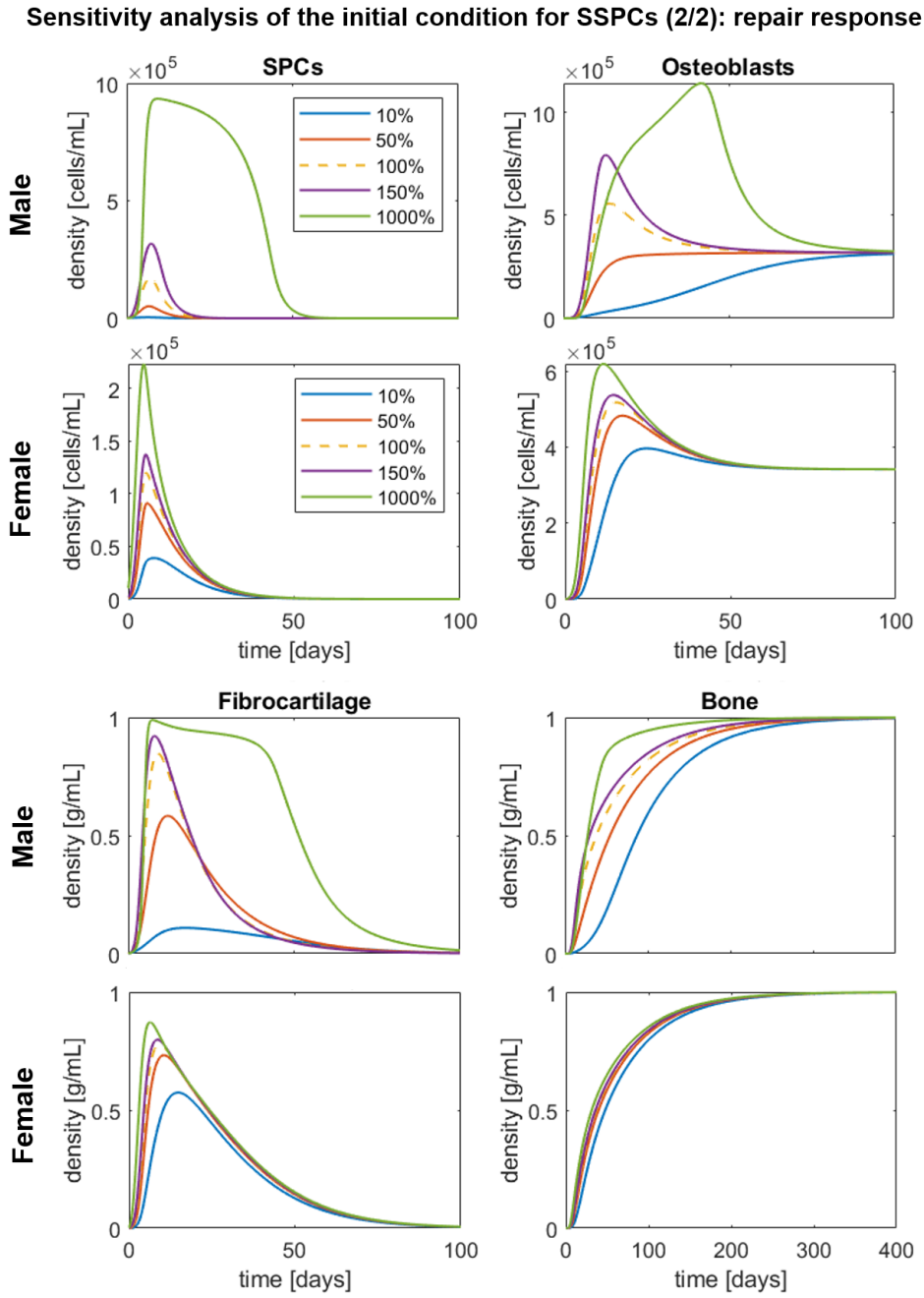


Figure S11: Influence of the initial condition for SSPCs on the repair phase.

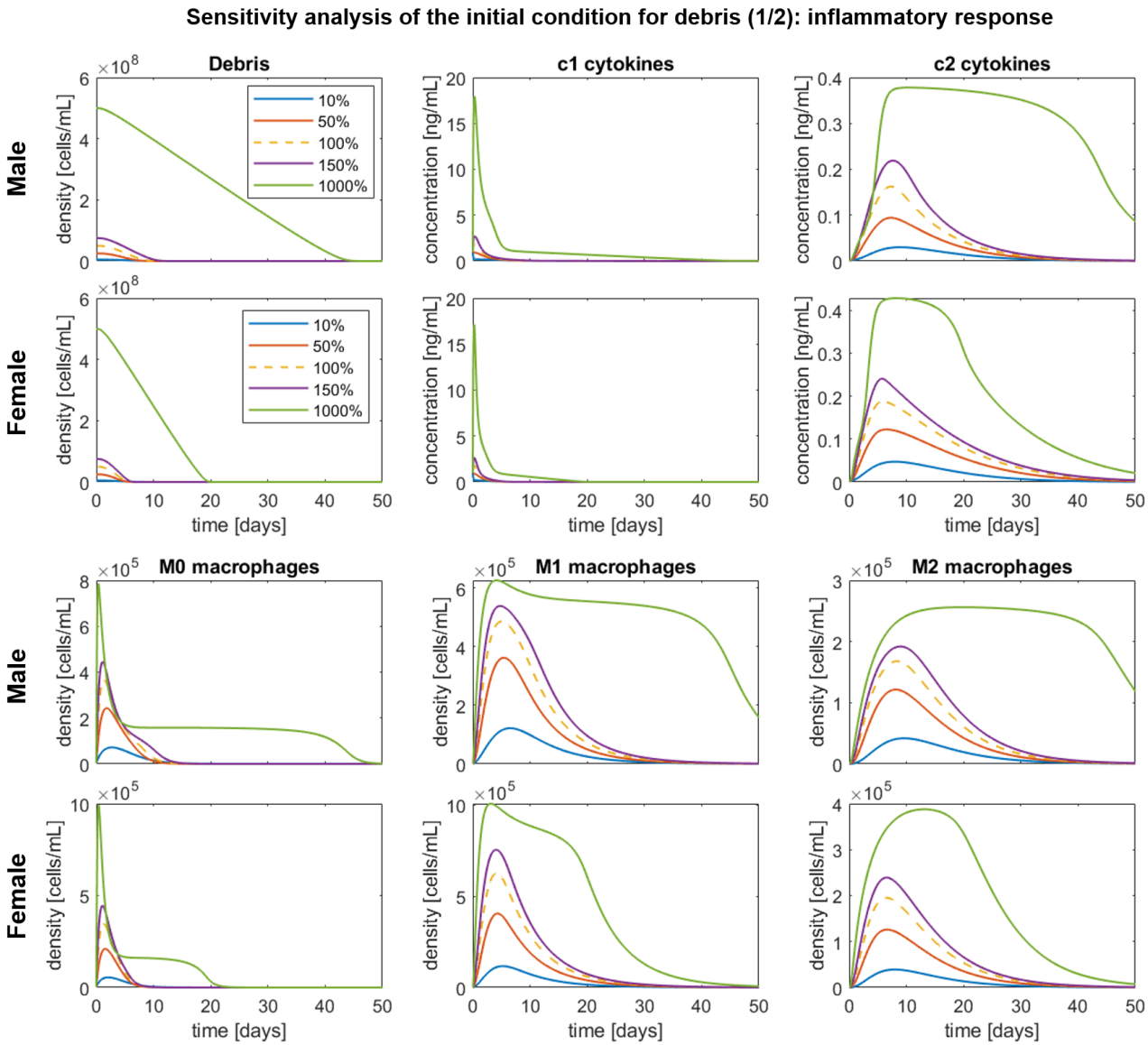


Figure S12: Influence of the initial condition for debris on the inflammatory phase.

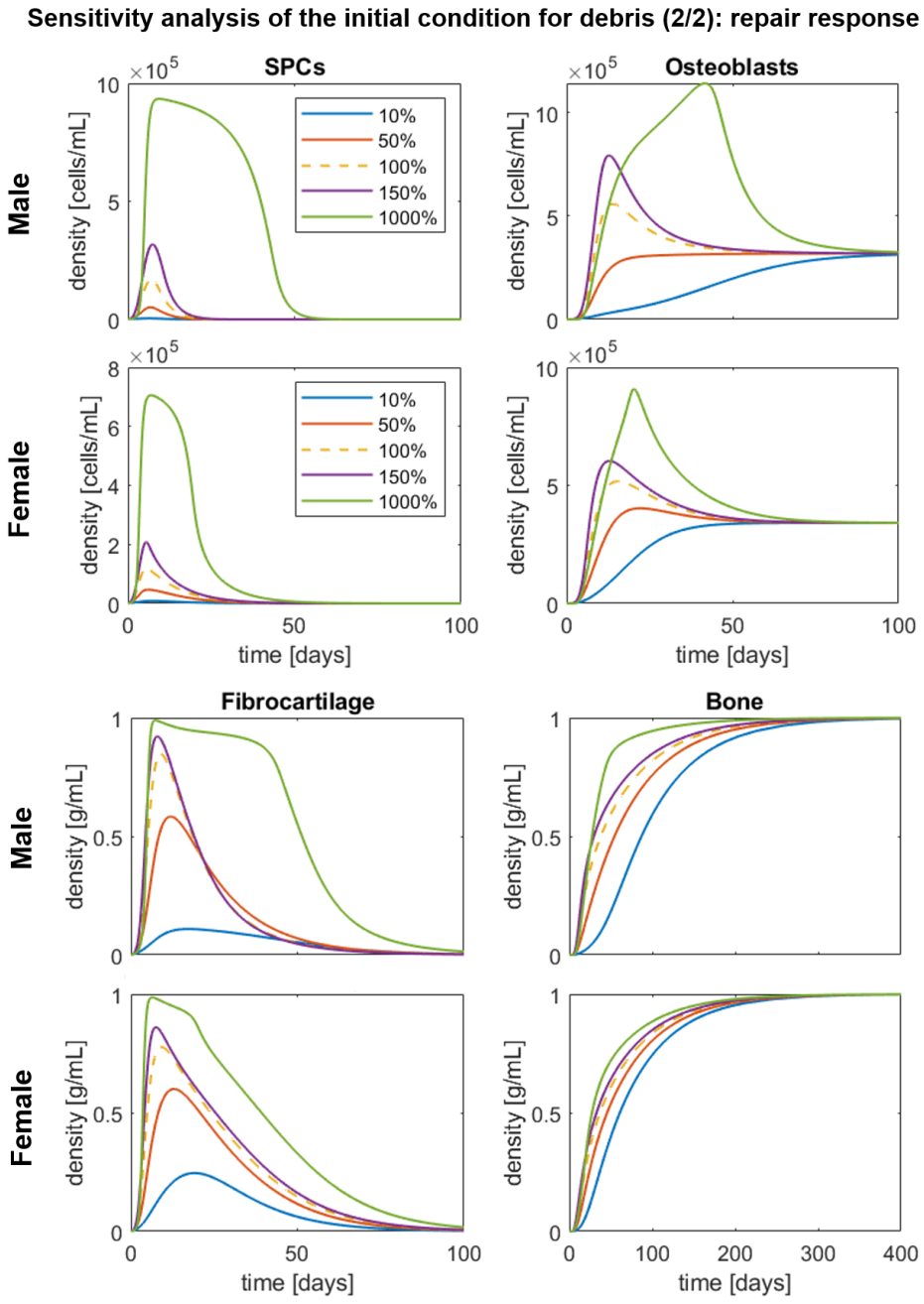


Figure S13: Influence of the initial condition for debris on the repair phase.

S4 Details on the full model results

S4.1 Output metrics

Tables S5 and S6 summarize the three output metrics calculated for each model outcome and for both male and female simulations: peak value, time-to-peak, and area under the curve (AUC). The AUC was calculated using the MATLAB `trapz()` function over the full 0 to 400 post-fracture day time range. To facilitate comparisons between the male and female models, Table S6 includes the male-to-female and female-to-male ratios for the AUC. These values provide a quantitative assessment of the differences in simulation outcomes between the sexes.

Additionally, we calculated the time at which bone density reaches 99% of its relative area: post-fracture day 285.748 for males and post-fracture day 286.055 for females. We also summed the AUCs of the three macrophage types, i.e. $M_{\text{tot}} = M_0 + M_1 + M_2$, to obtain the AUC of the total macrophage population. This resulted in $M_{\text{tot}} = 1.04 \times 10^7$ for males and $M_{\text{tot}} = 1.02 \times 10^7$ for females, yielding a male-to-female ratio of 1.01 and a female-to-male ratio of 0.99.

S4.2 Visual comparison of peak values

Fig. S14 facilitate direct visual comparison of peak values across cytokines (Fig. 6 B-C) and across macrophage (Fig. 6 D-F) and repair cells (Fig. 6 A-B) populations.

Table S5: Calculated peak values and times to peak for each model outcome, for both male and female cases.

	Peak value			Peak day	
Outcome	**Male**	**Female**	**Units**	**Male**	**Female**
D	5×10^7	5×10^7	cells/mL	0	0
M_0	3.65×10^5	3.46×10^5	cells/mL	1.39	1.24
M_1	4.86×10^5	6.26×10^5	cells/mL	5.08	4.2
M_2	1.68×10^5	1.95×10^5	cells/mL	8.24	6.45
c_1	1.8374	1.7882	ng/mL	0.29	0.21
c_2	0.1625	0.1878	ng/mL	7.41	5.84
C_s	1.71×10^5	1.2×10^5	cells/mL	7.03	5.46
C_b	5.58×10^5	5.17×10^5	cells/mL	13.95	15.59
m_f	0.847	0.7769	g/mL	9.08	9.19
m_b	0.9986	0.9991	g/mL	400	400

Table S6: Calculated area under the curve (AUC) and AUC ratios for each model outcome, for both male and female cases. The units for AUC are derived by dividing the outcome units (e.g. cells/mL) by days, resulting in units such as cells/(mL $\times$ day). The AUC ratios correspond to M/F (male-to-female) and F/M (female-to-male).

	AUC values			AUC ratios	
Outcome	**Male**	**Female**	**Units**	**M/F**	**F/M**
D	2.6×10^8	1.69×10^8	cells/(mL $\times$ days)	1.54	0.65
M_0	1.75×10^6	1.24×10^6	cells/(mL $\times$ days)	1.42	0.7
M_1	5.93×10^6	6.19×10^6	cells/(mL $\times$ days)	0.96	1.04
M_2	2.68×10^6	2.82×10^6	cells/(mL $\times$ days)	0.95	1.05
c_1	4.9274	3.0255	ng/(mL $\times$ days)	1.63	0.61
c_2	2.2203	3.3658	ng/(mL $\times$ days)	0.66	1.52
C_s	1.35×10^6	1.55×10^6	cells/(mL $\times$ days)	0.88	1.14
C_b	1.3×10^8	1.38×10^8	cells/(mL $\times$ days)	0.94	1.07
m_f	16.9309	23.4925	g/(mL $\times$ days)	0.72	1.39
m_b	340.4756	343.0612	g/(mL $\times$ days)	0.99	1.01

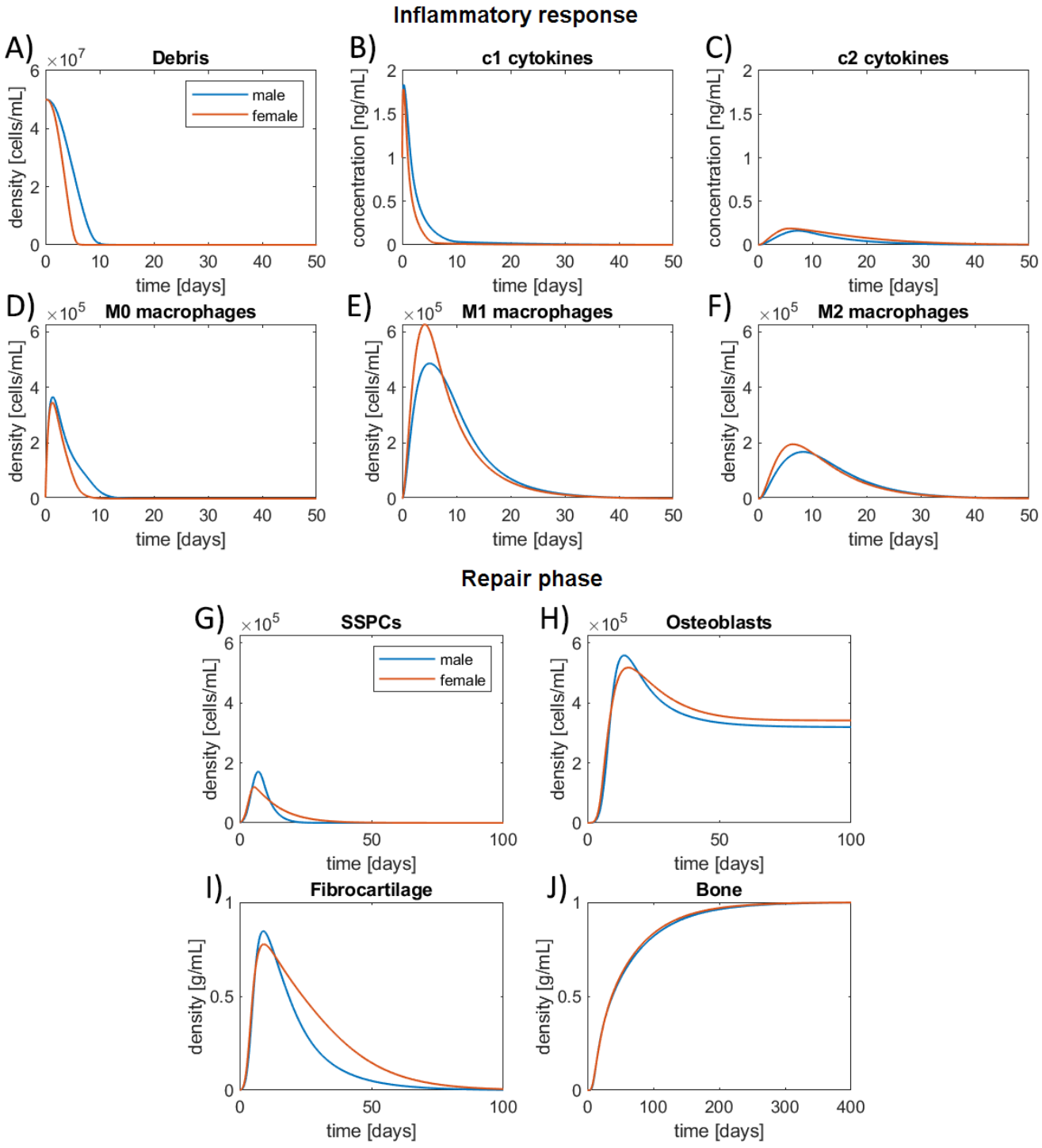


Figure S14: Predicted inflammatory and repair responses for the male (blue lines) and female (red lines) cases. The plots represent the temporal evolution of (A) debris density (D); (B) pro- (c_1) and (C) anti-inflammatory (c_2) cytokines concentration; (D) unactivated (M_0), (E) pro-inflammatory (M_1), and (F) anti-inflammatory (M_2) macrophage density; and (G) SSPC (C_s), (H) osteoblasts (C_b), (I) fibrocartilage (m_f), and (J) woven bone (m_b) density. Note that the y-axes are different per biological scale.

References

[1] J. B. Allen, C. Ludtka, and B. D. James. Sex as a biological variable in tissue engineering and regenerative medicine. *Annual Review of Biomedical Engineering*, 25:311–331, 2023.

[2] T. W. Andrew, L. S. Koepke, Y. Wang, M. Lopez, H. Steininger, D. Struck, T. Boyko, T. H. Ambrosi, X. Tong, Y. Sun, G. S. Gulati, M. P. Murphy, O. Marecic, R. Telvin, K. Schallmoser, D. Strunk, J. Seita, S. B. Goodman, F. Yang, M. T. Longaker, G. P. Yang, and C. K. Chan. Sexually dimorphic estrogen sensing in skeletal stem cells controls skeletal regeneration. *Nature Communications*, 13, 12 2022.

[3] D. M. Carp and Y. Liang. Universal or personalized mesenchymal stem cell therapies: Impact of age, sex, and biological source. *Cells*, 11(13), 2022.

[4] P. R. Crisostomo, M. Wang, C. M. Herring, T. A. Markel, K. K. Meldrum, K. D. Lillemoe, and D. R. Meldrum. Gender differences in injury induced mesenchymal stem cell apoptosis and vegf, tnf, il-6 expression: Role of the 55 kda tnf receptor (tnfr1). *Journal of Molecular and Cellular Cardiology*, 42:142–149, 1 2007.

[5] I. Decoene, H. Svitina, M. Belal Hamed, A. Economou, S. Stegen, F. P. Luyten, and I. Papantoniou. Callus organoids reveal distinct cartilage to bone transition mechanisms across donors and a role for biological sex. *Bone Research*, 13(1):41, 2025.

[6] M. Haffner-Luntzer, V. Fischer, and A. Ignatius. Differences in fracture healing between female and male c57bl/6j mice. *Frontiers in Physiology*, 12, 8 2021.

[7] O. Katsara, L. G. Mahaira, E. G. Iliopoulou, A. Moustaki, A. Antsaklis, D. Loutradis, K. Stefanidis, C. N. Baxevanis, M. Papamichail, and S. A. Perez. Effects of donor age, gender, and in vitro cellular aging on the phenotypic, functional, and molecular characteristics of mouse bone marrow-derived mesenchymal stem cells. *Stem Cells and Development*, 20:1549–1561, 9 2011.

[8] A. Kher, M. Wang, B. M. Tsai, J. M. Pitcher, E. S. Greenbaum, R. D. Nagy, K. M. Patel, G. M. Wairiuko, T. A. Markel, and D. R. Meldrum. Sex differences in the myocardial inflammatory response to acute injury. *Shock*, 23:1–10, 1 2005.

[9] S. L. Klein and K. L. Flanagan. Sex differences in immune responses. *Nature Reviews Immunology*, 16:626–638, 10 2016.

[10] S. S. Kurapaty and W. K. Hsu. Sex-based difference in bone healing: A review of recent pre-clinical literature. *Current Reviews in Musculoskeletal Medicine*, 15:651–658, 12 2022.

[11] G. Maged, M. A. Abdelsamed, H. Wang, and A. Lotfy. The potency of mesenchymal stem/stromal cells: does donor sex matter? *Stem Cell Research & Therapy*, 15(1):112, 2024.

[12] F. Mckinnirey, B. Herbert, G. Vesey, and S. McCracken. Immune modulation via adipose derived mesenchymal stem cells is driven by donor sex in vitro. *Scientific Reports*, 11, 12 2021.

[13] L. B. Meszaros, A. Usas, G. M. Cooper, and J. Huard. Effect of host sex and sex hormones on muscle-derived stem cell-mediated bone formation and defect healing. *Tissue Engineering - Part A*, 18:1751–1759, 9 2012.

[14] K. H. Molitoris, A. R. Balu, M. Huang, and G. S. Baht. The impact of age and sex on the inflammatory response during bone fracture healing. *JBMR Plus*, 3 2024.

[15] K. Nathan, L. Y. Lu, T. Lin, J. Pajarinen, E. Jämsen, J.-F. Huang, M. Romero-Lopez, M. Maruyama, Y. Kohno, Z. Yao, et al. Precise immunomodulation of the m1 to m2 macrophage transition enhances mesenchymal stem cell osteogenesis and differs by sex. *Bone & joint research*, 8(10):481–488, 2019.

[16] E. Ortona, M. T. Pagano, L. Capossela, and W. Malorni. The role of sex differences in bone health and healing. *Biology*, 12, 7 2023.

[17] L. M. Pennell, C. L. Galligan, and E. N. Fish. Sex affects immunity. *Journal of Autoimmunity*, 38, 5 2012.

[18] A. Saltelli, M. Ratto, T. Andres, F. Campolongo, J. Cariboni, D. Gatelli, M. Saisana, and S. Tarantola. *Global sensitivity analysis: the primer*. John Wiley & Sons, 2008.

[19] C. P. Schneider, M. G. Schwacha, and I. H. Chaudry. Impact of sex and age on bone marrow immune responses in a murine model of trauma-hemorrhage. *J Appl Physiol*, 102:113–121, 2007.

[20] P. Strube, M. Mehta, A. Baerenwaldt, J. Trippens, C. J. Wilson, A. Ode, C. Perka, G. N. Duda, and G. Kasper. Sex-specific compromised bone healing in female rats might be associated with a decrease in mesenchymal stem cell quantity. *Bone*, 45:1065–1072, 12 2009.

[21] B. D. Sui, J. Chen, X. Y. Zhang, T. He, P. Zhao, C. X. Zheng, M. Li, C. H. Hu, and Y. Jin. Gender-independent efficacy of mesenchymal stem cell therapy in sex hormone-deficient bone loss via immunosuppression and resident stem cell recovery. *Experimental and Molecular Medicine*, 50, 12 2018.

[22] M. Toya, J. Kushioka, H. Shen, T. Utsunomiya, H. Hirata, M. Tsubosaka, Q. Gao, S. K.-H. Chow, N. Zhang, and S. B. Goodman. Sex differences of nf-κb-targeted therapy for mitigating osteoporosis associated with chronic inflammation of bone. *Bone Joint Res*, 13:28–39, 2024.

[23] M. Ueno, N. Zhang, H. Hirata, D. Barati, T. Utsunomiya, H. Shen, T. Lin, M. Maruyama, E. Huang, Z. Yao, J. Y. Wu, S. Zwingenberger, F. Yang, and S. B. Goodman. Sex differences in mesenchymal stem cell therapy with gelatin-based microribbon hydrogels in a murine long bone critical-size defect model. *Frontiers in Bioengineering and Biotechnology*, 9, 10 2021.

[24] H. Zhang, A. Kot, Y. A. E. Lay, F. A. Fierro, H. Chen, N. E. Lane, and W. Yao. Acceleration of fracture healing by overexpression of basic fibroblast growth factor in the mesenchymal stromal cells. *Stem Cells Translational Medicine*, 6:1880–1893, 10 2017.